JOURNAL OF SOLID STATE CHEMISTRY 82, 203–215 (1989)

Synthesis, Crystal Structure, and Magnetism of $Fe_4(OH)_3(PO_4)_3$ and $V_4O(OH)_2(PO_4)_3$: Chains of M_2O_9 Dimers Connected by Hydroxyl Groups

C. C. TORARDI[1]

Central Research and Development Department,[2] E. I. du Pont de Nemours and Company, Experimental Station, Wilmington, Delaware 19880-0356

AND W. M. REIFF[1] AND L. TAKACS

Department of Chemistry, Northeastern University, Boston, Massachusetts 02115

Received December 22, 1988; in revised form June 5, 1989

The new compounds $Fe_4(OH)_3(PO_4)_3$ and $V_4O(OH)_2(PO_4)_3$ are prepared hydrothermally by reaction of Fe_2O_3 and V_2O_3 with aqueous H_3PO_4 solutions. X-ray powder diffraction shows that the two compounds have the same monoclinic structure. $Fe_4(OH)_3(PO_4)_3$ crystallizes with unit cell parameters a = 19.555(2), b = 7.376(1), c = 7.429(1) Å, and β = 102.26(1)° in the space group $C2/c$ with Z = 4. Dimers of face-sharing (nonequivalent) FeO_6 octahedra are interconnected by OH groups to form a double-chain of dimers extended along the c axis. Double chains are linked to one another by PO_4 tetrahedra that share corners with the octahedra. The Mössbauer spectrum of $Fe_4(OH)_3(PO_4)_3$ at 293 K exhibits two narrow width quadrupole doublets of equal intensity, with nearly identical isomer shifts and different quadrupole splittings: δ_1 = 0.407 mm/sec, δ_2 = 0.403 mm/sec, ΔE_1 = 0.657 mm/sec, ΔE_2 = 0.294 mm/sec. Low-temperature spectra indicate magnetic hyperfine splitting and three-dimensional magnetic order among the dimers at 86.7 ± 0.2 K. Below the ordering temperature, the spectrum consists of two equal intensity sextets with saturation hyperfine fields (4.2 K) of 52.9 and 49.1 T, respectively. The temperature dependence of the magnetic susceptibility confirms that ordering occurs at 87 ± 0.5 K with an abrupt rise to a high-moment ferromagnetic state. Above the ordering temperature, the susceptibility data exhibits a broad maximum at about 125 K characteristic of antiferromagnetically coupled dimers. The moment vs temperature behavior of $V_4O(OH)_2(PO_4)_3$ also shows antiferromagnetic exchange that is likely pairwise in nature, analogous to the iron compound, in view of the broad maximum in the susceptibility data at ~150 K.

Introduction

The complex phosphates and hydroxyphosphates of iron(III), particularly as prepared by reaction of iron phases with orthophosphoric acid, continue to be of importance in a number of contexts. They are significant in corrosion inhibition and passivation of metal surfaces (*1*). They are also important in any consideration of the reactions of iron compounds contained in various soils with phosphate fertilizers (*2*). Needless to say they are also of interest

[1] To whom correspondence may be addressed.
[2] Contribution No. 5021.

0022-4596/89 $3.00

from a basic research point of view. These compounds present a variety of complex network structures and thus basic magnetic behavior and are a challenge to complete characterization. This is evident in a recent study of the complex phosphate oxonium iron(III) orthophosphate hydrate, wherein detailed comparisons are made to a host of other phosphate compounds of iron(II) and iron(III) (*3*).

In the present study, one has a complex phosphate with a novel combination of an extended network structure but with discernible structural dimers such that the intradimer and interdimer magnetic interactions can be conveniently studied by magnetic susceptibility and Mössbauer spectroscopy techniques. The observation of clearly separable pairwise and extended three-dimensional antiferromagnetic interactions in the same compound is not that common. Another system which we have recently studied and for which we have found similar behavior is a new polymorph of anhydrous ferric arsenate (*4*). The study of such systems potentially allows for a better understanding of the competitive interactions that lead to the overall three-dimensional magnetic structure and ground state. It is with this in mind that we have pursued a detailed study of the title compound. In this work, we also present structural and magnetic susceptibility characterization of a related isomorphous mixed-valence vanadium system.

Experimental

Synthesis

$Fe_4(OH)_3(PO_4)_3$. This compound was prepared under hydrothermal conditions. Typical reactions consisted of sealing 0.8 to 1.5 g Fe_2O_3 (Alpha 99.9) and 4 to 5 ml of 3.7 to 7.4 *M* H_3PO_4 solution in a gold tube (15 cm in length × 1 cm in diameter) and heating the mixture at 700°C and 3 kbar pressure for 12 hr. The reactions were then slowly cooled at a rate of 25°C/hr to 400°C. The green polycrystalline product was washed with distilled water, rinsed with acetone, and dried in air. Crystals of $Fe_4(OH)_3(PO_4)_3$ were obtained by using concentrated (14.7 *M*) H_3PO_4 solution. However, another new orthorhombic ferric phosphate, $Fe_2(P_2O_7)(HPO_4)$ (*5*), also crystallized from these reactions but was easily separated from $Fe_4(OH)_3(PO_4)_3$ because of the differences in color, crystal habit, and size.

The title compound was initially characterized by chemical analyses, which gave an Fe/P molar ratio of 1.36, and by thermogravimetric analysis in air. $Fe_4(OH)_3(PO_4)_3$ begins to decompose at ~550°C and exhibits a weight loss of 4.7% at 1000°C (calculated 4.8%). The decomposition products were identified by X-ray powder diffraction as $FePO_4$ and Fe_3PO_7.

$V_4O(OH)_2(PO_4)_3$. A mixed-valence vanadium analog isostructural to the iron compound was also synthesized. A brown phase, $V_4O(OH)_2(PO_4)_3$, containing vanadium in a +3.25 average oxidation state, was made, using V_2O_3 and excess 3.7 *M* H_3PO_4 solution in the manner described above for the ferric compound. The X-ray powder diffraction pattern for this product was essentially the same as that of the iron phase. $V_4O(OH)_2(PO_4)_3$ was further characterized by chemical analyses which gave a V/P molar ratio of 1.35. Thermogravimetric analysis to 1000°C under N_2 showed incipient weight loss at ~550°C and a 3.3% total weight loss that compares quite well with the calculated value of 3.3%. A TGA analysis performed under an O_2 atmosphere showed a 7.1% weight increase at 600°C. This value also compared well with that calculated for combined H_2O loss and oxidation of vanadium to the +5 state, 7.05%. Above 700°C, the oxidized material exhibited a decrease in weight due to the loss of

oxygen as is known to occur for V^{5+} compounds.

X-Ray Powder Diffraction

X-ray powder diffraction data for the two new compounds were collected with a Philips APD 3600-02 diffractometer, automated with a Data General Nova computer. The unit was equipped with a long, fine focus Cu tube, a theta-compensating slit, and a graphite diffracted-beam monochromator ($\lambda = 1.5418$ Å). Silicon powder was used as an internal standard. Lattice parameters for C-centered monoclinic cells were refined by a least-squares procedure. The X-ray powder diffraction patterns for both compounds were found to be essentially identical. A comparison of the unit cell parameters for the two compounds is given in Table I. The indexed X-ray powder diffraction pattern of $Fe_4(OH)_3(PO_4)_3$ recorded at room temperature is given in Table II.

Single-Crystal X-Ray Diffraction[3]

Information on the single-crystal X-ray data collection and structural refinement of $Fe_4(OH)_3(PO_4)_3$ is given in Table III. The data were treated for Lorentz and polarization effects and then averaged in $2/m$ symmetry. Heavy atom positions were found by using MULTAN (*6*). Oxygen and hydrogen atom positions were located from difference Fourier maps. A correction for absorption was applied using DIFABS (*7*) after a full isotropic refinement was made. The largest peak present in a final difference Fourier map was 0.40 e/Å^3.

Atomic positional and thermal parameters for $Fe_4(OH)_3(PO_4)_3$ are given in Tables IVa and IVb and important interatomic distances and angles are listed in Table V. Structural figures were drawn with the assistance of the ORTEP program (*8*).

[3] All crystallographic calculations were performed on a VAX 11/780 computer using a system of programs developed by J. C. Calabrese.

TABLE I

COMPARISON OF UNIT CELL PARAMETERS FOR $Fe_4(OH)_3(PO_4)_3$ AND $V_4O(OH)_2(PO_4)_3$

Compound	a (Å)	b (Å)	c (Å)	β (°)
$Fe_4(OH)_3(PO_4)_3$[a]	19.554(3)	7.395(1)	7.439(1)	102.45(1)
	19.555(2)	7.376(1)	7.429(1)	102.26(1)
$V_4O(OH)_2(PO_4)_3$	19.528(5)	7.404(2)	7.383(2)	101.94(2)

[a] The first line is from X-ray powder data; the second line is from single-crystal data.

Mössbauer Spectroscopy

Mössbauer spectra were recorded between 4.2 K and room temperature using conventional constant-acceleration Mössbauer spectrometers. At low temperatures, both the source and the absorber were cooled with the source being driven vertically. An exchange gas-type cryostat (Janis Research, Wilmington, Massachusetts) and liquid nitrogen as the cryogen were used between 48 and 100 K. Above 78 K, the temperature was controlled with a DTC-500 temperature controller (Lake Shore Cryotronics Co., Westerville, Ohio) connected to a silicon diode and a 10-ohm heater. Below the standard boiling point of nitrogen, the vapor pressure above the nitrogen bath was also controlled. Some temperatures were reached with the nitrogen frozen. The spectrum at 4.2 K was recorded in a flow-type helium cryostat (Janis Research). The temperature of the sample was measured by calibrated silicon diodes driven by a 10-μA constant current source (Lake Shore Cryotronics Co.). The absolute precision of the temperature measurement was about ± 0.2 K and the temperature control close to the ordering temperature was an order of magnitude better.

The Mössbauer spectra were fitted using Lorentzians and evaluation programs of local origin. Spectra in the magnetically ordered regime were fitted to two sextets with identical total intensities but different hyperfine fields, isomer shifts, and quadrupole

TABLE II

X-RAY POWDER DIFFRACTION DATA FOR $Fe_4(OH)_3(PO_4)_3$

2θ	I(obs)	$h\ k\ l$	d(obs)	d(calc)	2θ	I(obs)	$h\ k\ l$	d(obs)	d(calc)
12.873	7	1 1 0	6.876	6.896	46.323	1	−9 1 2	1.960	1.960
17.024	5	−1 1 1	5.208	5.208			−7 1 3		1.969
18.399	7	3 1 0	4.822	4.824	47.960	6	−5 3 2	1.897	1.897
		1 1 1		4.817	48.801	7	9 1 1	1.866	1.865
18.569	6	4 0 0	4.778	4.774			−6 2 3		1.868
20.419	3	−3 1 1	4.349	4.360			−10 0 2		1.864
23.735	9	3 1 1	3.749	3.746			−2 0 4		1.859
24.465	2	0 0 2	3.638	3.632			6 2 2		1.873
		−2 0 2		3.667	49.306	14	0 4 0	1.848	1.849
25.880	20	2 2 0	3.443	3.448			8 2 1		1.850
26.260	9	5 1 0	3.394	3.393	49.907	8	7 3 0	1.827	1.829
26.826	100	−1 1 2	3.323	3.322			8 0 2		1.822
		−5 1 1		3.328			−4 0 4		1.834
		0 2 1		3.295	50.212	9	0 0 4	1.817	1.816
27.776	32	−2 2 1	3.212	3.213			2 4 0		1.815
28.026	26	6 0 0	3.184	3.182			5 1 3		1.814
		2 0 2		3.175	50.703	3	−3 1 4	1.800	1.799
		−3 1 2		3.160	52.435	8	−1 3 3	1.745	1.745
31.052	1	5 1 1	2.880	2.871			2 4 1		1.744
31.483	1	−4 2 1	2.842	2.845			−5 1 4		1.746
32.488	1	−5 1 2	2.756	2.757			−6 0 4		1.748
33.153	1	−6 0 2	2.702	2.699			−9 1 3		1.748
		3 1 2		2.697			−7 3 2		1.737
34.019	7	4 0 2	2.635	2.630	53.131	2	4 4 0	1.724	1.724
34.519	29	4 2 1	2.598	2.596			1 1 4		1.723
		−2 2 2		2.604			−10 2 1		1.727
		0 2 2		2.591			−11 1 1		1.728
		−7 1 1		2.583	53.356	2	2 0 4	1.717	1.717
36.771	5	1 3 0	2.444	2.445			7 3 1		1.716
		−4 2 2		2.440			5 3 2		1.715
37.251	7	6 2 0	2.414	2.412	54.167	1	11 1 0	1.693	1.690
		−6 2 1		2.410			10 2 0		1.697
		2 2 2		2.409			1 3 3		1.697
37.606	5	8 0 0	2.392	2.387	55.203	50	−10 2 2	1.664	1.664
38.457	3	−1 1 3	2.341	2.342	55.333	47	−2 2 4	1.660	1.661
		−1 3 1		2.337	56.710	5	−8 0 4	1.623	1.624
39.192	15	3 3 0	2.299	2.299			−9 3 1		1.627
		1 3 1		2.298	57.421	64	7 1 3	1.605	1.604
39.608	15	7 1 1	2.275	2.274			3 3 3		1.606
		5 1 2		2.272			−4 4 2		1.607
40.378	2	1 1 3	2.234	2.231			9 3 0		1.608
		−8 0 2		2.227	57.581	30	6 4 0	1.601	1.599
		−3 3 1		2.242			−6 4 1		1.598
41.394	8	−6 2 2	2.181	2.180			2 4 2		1.598
		−5 1 3		2.178	57.997	21	12 0 0	1.590	1.591
		6 2 1		2.185			−12 0 2		1.589
		6 0 2		2.173	58.157	14	10 2 1	1.586	1.586
43.411	1	−9 1 1	2.084	2.079			4 0 4		1.587
44.086	23	−1 3 2	2.054	2.055			6 2 3		1.584
		−5 3 1		2.056			−6 2 4		1.580
		−2 2 3		2.058	59.754	3	−11 1 3	1.548	1.546
44.347	20	9 1 0	2.043	2.039			7 3 2		1.546
44.677	12	−8 2 1	2.028	2.029					
		0 2 3		2.026					
		3 1 3		2.035					

Plus 18 lines to $d = 1.35$

TABLE III

SUMMARY OF CRYSTAL DATA, COLLECTION DATA, AND REFINEMENT OF THE STRUCTURE $Fe_4(OH)_3(PO_4)_3$

Dimensions (mm)	0.20 × 0.23 × 0.27
Diffractometer	CAD4
Radiation	Mo$K\alpha$
Monochromater	Graphite
Formula weight	559.3
Crystal system	Monoclinic
Space group	$C2/c$
Cell constants	a = 19.555(2) Å
	b = 7.376(1) Å
	c = 7.429(1) Å
	β = 102.26(1)°
Calc. density (g · cm^{-3})	3.55
Scan mode	ω
2θ range	0–60°
Octants	+++, −++, +−+, ++−
μ (cm^{-1})	59.9
Absorption correction	DIFABS[a]
Total reflections	5395
Independent reflections	1373 ($I > 3\sigma$)
Data/parameters	12.7
R	0.019
R_w	0.029

[a] Reference (7).

TABLE IVa

POSITIONAL[a] AND THERMAL PARAMETERS FOR THE ATOMS OF $Fe_4(OH)_3(PO_4)_3$

Atom	x	y	z	B (Å^2)[b]
Fe(1)	0.83056(2)	0.51257(4)	0.64736(4)	0.5(1)′
Fe(2)	0.92443(2)	0.22328(4)	0.84415(4)	0.5(1)′
P(1)	0.00	0.6151(1)	0.75	0.4(1)′
P(2)	0.83132(3)	0.86501(7)	0.91481(7)	0.5(1)′
O(1)	0.00	0.1225(3)	0.75	0.9(1)′
O(2)	0.9371(1)	0.4920(2)	0.7603(2)	0.9(1)′
O(3)	0.8365(1)	0.6272(2)	0.4021(2)	0.7(1)′
O(4)	0.8134(1)	0.7411(2)	0.7472(2)	1.0(1)′
O(5)	0.7662(1)	0.9660(2)	0.9385(2)	1.1(1)′
O(6)	0.8578(1)	0.7451(2)	0.0868(2)	0.8(1)′
O(7)	0.0192(1)	0.7342(3)	0.9178(2)	1.2(1)′
O(8)	0.8881(1)	0.9975(2)	0.8959(3)	1.1(1)′
H(1)	0.803(2)	0.716(5)	0.385(5)	1.5(7)
H(2)	0.00	0.019(11)	0.75	6.6(23)

[a] Space group $C2/c$ (No. 15).

[b] B_{equiv} listed for Fe, P, and O.

shifts (assuming that the quadrupole interaction is a small perturbation of the magnetic hyperfine interaction). The width of the lines belonging to the same sextet was assumed to be equal, but the two sextets were allowed to have different widths. The intensity ratio $I_1 : I_2 : I_3$ was a fitted parameter, but it was assumed to be the same for the two sextets. The validity of these conditions was confirmed by fitting the well-resolved spectra recorded at the lowest temperatures under different conditions. The application of any more constraint decreased the quality of the fit (increased the χ^2 value) significantly. On the other hand, dropping any of the above constraints increased the correlations between the fitted parameters without a significant improvement of the quality of the fit. This system of constraints was used for all the magnetically split spectra for consistency even where the overlap of the lines made the comparison of different fitting conditions impossible. The spectra in the paramagnetic temperature region were fitted to two symmetrical quadrupole doublets with equal intensities (corresponding to the two equally intense sextets at lower temperatures). Although different line assignments are possible, the only physically reasonable

TABLE IVb

ANISOTROPIC THERMAL PARAMETERS[a] FOR THE ATOMS OF $Fe_4(OH)_3(PO_4)_3$

Atom	B_{11}	B_{22}	B_{33}	B_{12}	B_{13}	B_{23}
Fe(1)	0.48(1)	0.52(1)	0.50(1)	0.04(1)	0.11(1)	−0.01(1)
Fe(2)	0.53(1)	0.51(1)	0.53(1)	−0.02(1)	0.11(1)	0.02(1)
P(1)	0.38(3)	0.44(3)	0.48(3)	0	0.06(2)	0
P(2)	0.49(2)	0.42(2)	0.45(2)	0.02(1)	0.09(1)	0.02(1)
O(1)	0.9(1)	0.6(1)	1.2(1)	0	0.5(1)	0
O(2)	0.49(5)	0.77(6)	1.39(7)	−0.08(4)	0.18(5)	0.25(5)
O(3)	0.61(5)	0.80(6)	0.65(6)	0.08(4)	0.25(5)	0.10(5)
O(4)	1.72(7)	0.68(6)	0.63(6)	0.19(5)	0.09(5)	−0.18(5)
O(5)	0.65(6)	1.29(7)	1.18(6)	0.25(5)	0.05(5)	−0.35(5)
O(6)	0.97(6)	0.67(5)	0.57(5)	−0.17(5)	−0.07(5)	0.17(4)
O(7)	1.07(6)	1.54(7)	0.95(6)	0.23(5)	−0.13(5)	−0.65(5)
O(8)	0.94(6)	0.87(6)	1.54(7)	−0.18(5)	0.39(5)	0.34(5)

[a] $\exp[-0.25(B_{11}h^2a^{*2} \ldots + 2(B_{12}hka^*b^* \ldots))]$.

TABLE V

SELECTED INTERATOMIC DISTANCES (Å) AND ANGLES (°) FOR $Fe_4(OH)_3(PO_4)_3$

Fe(1)–O(2)	2.080(2)	P(1)–O(2)	1.544(2) (2×)
Fe(1)–O(3)	2.136(2)	P(1)–O(7)	1.506(2) (2×)
Fe(1)–O(3)a	2.034(2)	P(2)–O(4)	1.524(2)
Fe(1)–O(4)	1.900(2)	P(2)–O(5)	1.518(2)
Fe(1)–O(5)	1.895(2)	P(2)–O(6)	1.550(2)
Fe(1)–O(6)	2.049(2)	P(2)–O(8)	1.507(2)
Fe(2)–O(1)	1.914(1)	O(1)–H(2)	0.76(8)
Fe(2)–O(2)	2.108(2)	O(3)–H(1)	0.91(4)
Fe(2)–O(3)	2.162(2)	Fe(1)–Fe(2)	2.987(1)
Fe(2)–O(6)	2.086(2)		
Fe(2)–O(7)	1.901(2)		
Fe(2)–O(8)	1.882(2)		
Fe(2)–O(1)–Fe(2)	134.3(1)		
Fe(1)–O(2)–Fe(2)	91.0(1)		
Fe(1)–O(3)–Fe(2)	88.0(1)		
Fe(1)–O(3)a–Fe(1)	126.2(1)		
Fe(1)–O(3)a–Fe(2)	126.1(1)		
Fe(1)–O(6)–Fe(2)	92.5(1)		

one is that with essentially identical isomer shifts and somewhat different quadrupole splittings. All these fitting conditions are fully in accord with the crystal structure showing two slightly different ferric iron sites. The unresolved spectrum taken the closest to the transition temperature (86.67 K) was fitted to the sum of a symmetrical doublet and a sextet with a fixed 3 : 2 : 1 intensity ratio.

Susceptibility Measurements

Susceptibility measurements (*9*) were performed from just below the transition temperature to room temperature using a Faraday balance. The applied fields ranged from 500 Oe to 5 kOe. A flow-type cryostat (Janis Research) using nitrogen as the cryogen was used to cool the sample. The sample temperature was read by a calibrated silicon diode with a precision of 0.2 K while temperature control was achieved using a Lake Shore Cryotronics DTC-500 set point controller connected to a gallium arsenide diode thermometer and a 10-ohm heater.

Results and Discussion

Structural Description

The structure of $Fe_4(OH)_3(PO_4)_3$ contains face-sharing pairs of FeO_6 octahedra. One such unit is shown in Fig. 1. The Fe–Fe separation within the dimer is 2.987 Å. Average Fe–O bond lengths of 2.016 Å for Fe(1) and 2.009 Å for Fe(2) compare well with the sum of ionic radii (*10*), 2.005 Å. Hydrogen atoms are bonded to oxygen atoms O(1) and O(3), and these OH groups, which serve as the connections between individual dimers, bond to iron atoms in neighboring units. All the other oxygen atoms in the dimeric unit are shared with PO_4 tetrahedra.

Dimeric units are interconnected in a zigzag fashion by atoms O(3) to form strings of dimers running along the *c* axis (Fig. 2a). Two such strings are linked via the O(1) atoms to form a double chain of dimers (Fig. 2b) possessing a narrow tunnel that runs the length of the double chain. Figure 3 shows how the tunnel-shaped double chains are oriented parallel to each other along the *c* axis. There are no direct Fe–O–Fe bridges between the double chains. The shortest intrachain Fe–Fe distance between dimers is 3.528 Å across the chain and 3.719 Å along the chain. Phosphorous atoms, P(1), are located in the tunnels of the double chains in tetrahedral coordina-

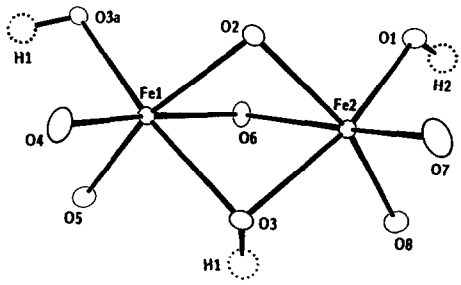

FIG. 1. One of the face-sharing pairs of FeO_6 octahedra in $Fe_4(OH)_3(PO_4)_3$.

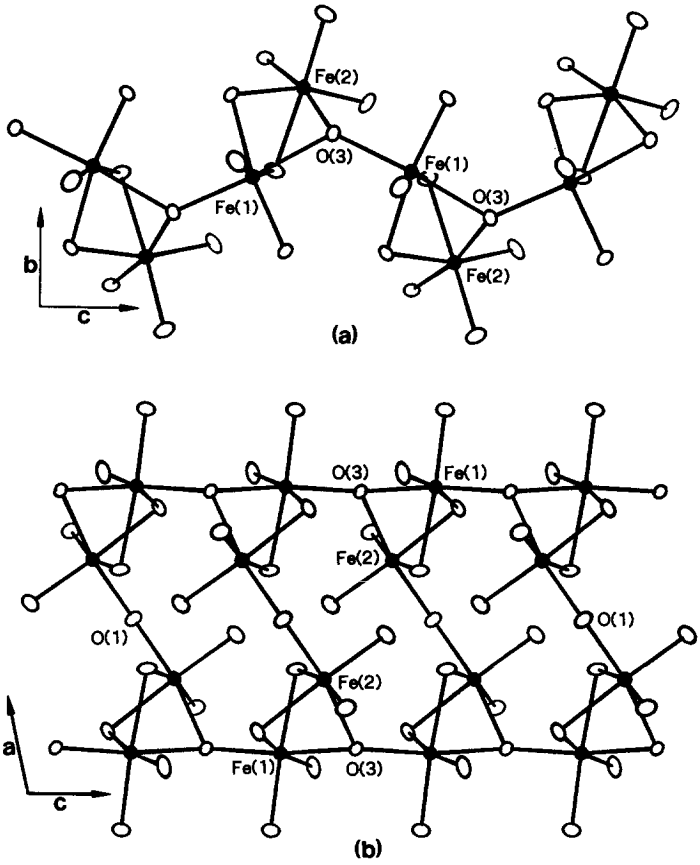

FIG. 2. (a) Strings of Fe_2O_9 dimers running along the c axis for $Fe_4(OH)_3(PO_4)_3$. Fe atoms are shaded. (b) A double chain of dimers oriented along c. Fe atoms are shaded.

tion with oxygen, and these atoms also interconnect the dimers of the chain.

Individual double chains are linked by phosphorous atoms, P(2), via Fe–O–P–O–Fe connections (i.e., corner-sharing of octahedra with tetrahedra). Each P(2) atom bridges three iron–oxygen double chains. The shortest *interchain Fe–Fe* distances are 4.695 Å between chains stacked in the b direction and 4.905 Å between chains in the [110] direction (Fig. 3).

The average P–O bond lengths within the two types of tetrahedra (Table V) are the same at 1.525 Å and agree quite well with the sum of ionic radii (*10*), 1.53 Å. Oxygen atoms O(4), O(5), O(7), and O(8) are two coordinate and are bonded to one Fe and one P atom. Atoms O(2) and O(6) are three coordinate being bonded to two Fe atoms and one P atom. O(1) and O(3), the intrachain links between the face-sharing iron dimers, are three and four coordinate, respectively. O(1) is bonded to two Fe atoms and one H atom, while O(3) is connected to three Fe atoms and one H atom.

The structure of $Fe_4(OH)_3(PO_4)_3$ is related to that of the mineral barbosalite, $Fe_3(OH)_2(PO_4)_2$, which contains mixed-valent iron (*11*). However, the latter compound displays groups of three FeO_6 octahedra that share faces. Analogous to the present compound, the trimers in barbosa-

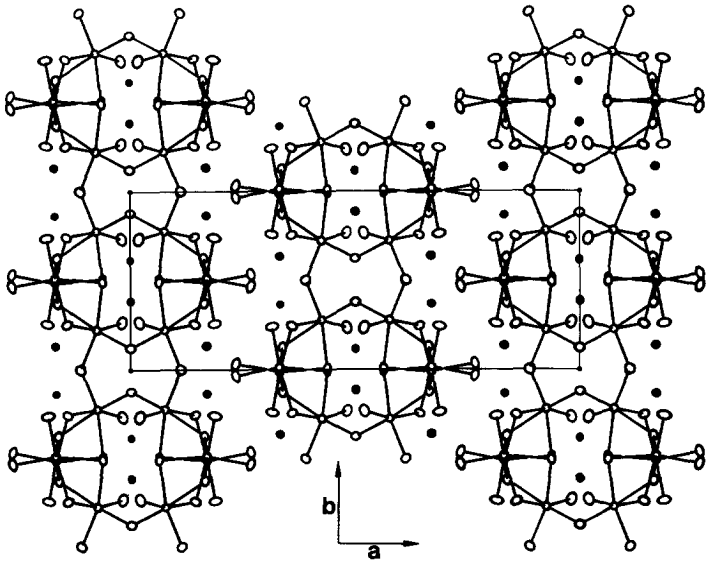

FIG. 3. Arrangement of double chains of Fe_2O_9 dimers parallel to each other along the c axis. P atoms are shaded. Only Fe–O bonds are shown.

lite are linked through corner-shared hydroxyl groups and through corner-shared oxygen atoms of the phosphate groups. Another mixed-valence basic ion phosphate is iron lazulite with approximate composition $Fe_7(OH)_4(PO_4)_4$ (*12*). This material possesses infinite chains of face-shared FeO_6 octahedra interconnected by corner-shared OH groups. A common feature found in all of these compounds is an OH group that bridges three iron atoms. This hydroxyl anion is one of the three face-shared anions between two octahedra (O(3)–H(1) in Fig. 1), and serves as the corner-shared link to another octahedron. In addition to this type of hydroxyl unit, the present compound also contains another OH group (O(1)–H(2) in Fig. 1) that forms a bridge between two iron atoms.

Isostructural with $Fe_4(OH)_3(PO_4)_3$ is the new vanadium phase, $V_4O(OH)_2(PO_4)_3$, whose preparation was described above. It is a mixed-valence phase formally containing $V^{3.25+}$ (three V^{3+} and one V^{4+}). However, further work needs to be done on this compound in order to determine whether the oxidation states are statically or dynamically disordered. Presumably, the missing proton in $V_4O(OH)_2(PO_4)_3$, relative to $Fe_4(OH)_3(PO_4)_3$, is from atom O(1) in Fig. 1. This proton resides on a special position of space group $C2/c$ in the ferric compound. The remaining protons, which are located on general positions, make up the triply bridging OH groups that were discussed above.

Mössbauer Measurements

The room-temperature Mössbauer spectrum (Fig. 4) can be well described by the overlap of two symmetric doublets with identical intensities. The isomer shifts of the two doublets are nearly identical (0.407 and 0.403 mm/sec), but the quadrupole splittings differ by more than a factor of two (0.657 and 0.295 mm/sec, respectively). The linewidth after deconvolution is 0.27 mm/sec, close to the linewidth (0.25 mm/sec) obtained for a thin iron calibration foil. This deconvolution is in accord with the

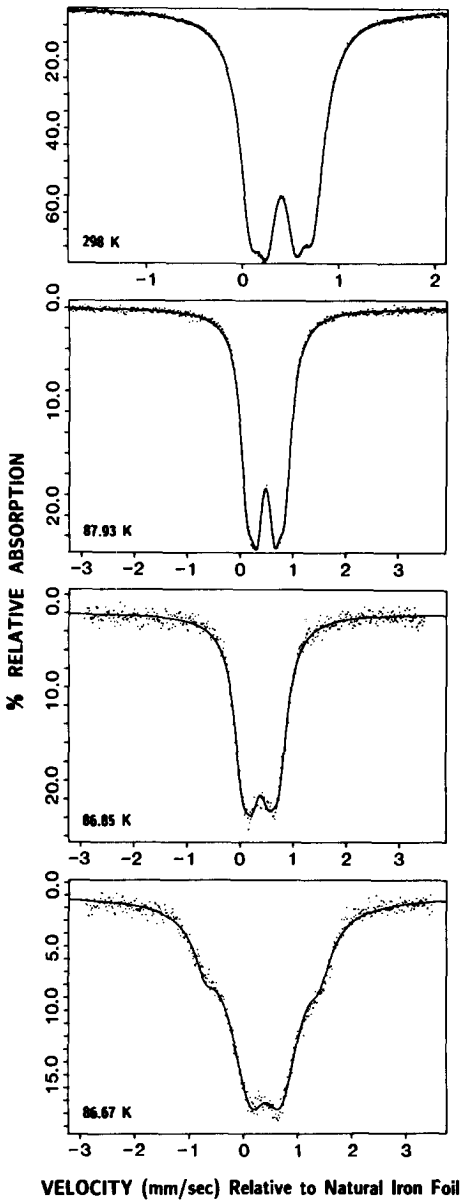

FIG. 4. Mössbauer spectra of $Fe_4(OH)_3(PO_4)_3$ above and close to the ordering temperature.

presence of two equally populated six-coordinate high-spin ferric sites of different local coordination symmetry. Both of the high-spin ferric ions are surrounded by an octahedron of oxygen atoms explaining the very close isomer shifts. However, their deviations from perfect octahedral symmetry must be somewhat different so as to explain the widely different quadrupole splittings. The octahedra around the Fe(1) and Fe(2) sites are in fact clearly rather different. Three out of the six oxygen neighbors (O(2), O(3), and O(6)) are shared between an Fe(1) and an Fe(2) atom. The average distances between the iron atom and these three oxygen neighbors is 2.088 Å for Fe(1) and, somewhat larger, 2.119 Å for Fe(2). The other three oxygen neighbors are slightly closer to the iron atoms, the average distances being 1.943 Å for Fe(1) and, smaller, 1.899 Å for Fe(2). These data indicate that the octahedron around Fe(2) is more distorted and it is likely the site corresponding to the larger quadrupole splitting, although an estimation (lattice summation calculation) of the electric field gradient would be necessary to make a more definitive site assignment. As expected for high-spin Fe^{3+}, the quadrupole splitting is only slightly temperature dependent. At 87.9 K, 1 K above the magnetic ordering temperature, the quadrupole splittings of the two doublets are 0.708 and 0.325 mm/sec, respectively.

The Mössbauer spectra indicate long-range magnetic ordering at 86.7 ± 0.2 K. Above the ordering temperature, the linewidth of the paramagnetic doublet is independent of the temperature until 87.03 K. The first sign of approaching magnetic ordering is a 0.03 mm/sec increase of the linewidth at 86.85 K (Fig. 4). The presence of long-range (three-dimensional) magnetic ordering is already evident in the spectrum measured at 86.67 K (Fig. 4) while the spectrum recorded at 86.13 K already exhibits a fully resolved magnetic hyperfine pattern (Fig. 5). This spectrum was fitted to two sextets assuming that the quadrupolar interaction is a small perturbation of the magnetic hyperfine interaction.

The spectra recorded at lower temperatures are the superpositions of two well-re-

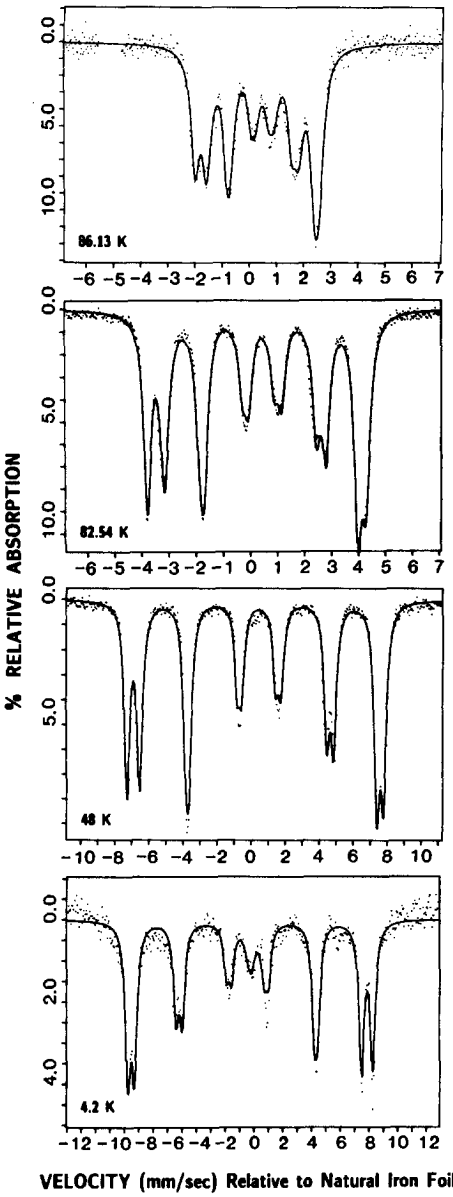

FIG. 5. Typical low-temperature Mössbauer spectra of $Fe_4(OH)_3(PO_4)_3$.

solved asymmetric sextets (Fig. 5). Two different line assignments are possible, resulting in approximately equal χ^2 values. However, only one of them corresponds to two sextets with nearly identical isomer shifts, the other gives different and strongly temperature-dependent isomer shifts and physically unreasonable quadrupole splittings. The Brillouin-like-functional temperature dependence of the hyperfine fields (H_n) obtained for the two sextets is presented in Fig. 6. The saturation values measured at 4.2 K are 529 and 491 kOe, respectively, where it is tempting perhaps to assign the smaller value of H_n to a more covalent Fe site. As the temperature increases, the lower hyperfine field decreases somewhat faster than the higher one.

The quadrupole shifts of the two sextets are practically temperature independent. (The average values are -0.135 mm/sec for the higher field and 0.027 mm/sec for the lower field sextet, respectively.) This indicates that no change in the angle between the direction of the electric field gradient and the hyperfine field occurs; i.e., the easy magnetization direction remains unchanged, and there is no obvious spin reorientation transformation. In systems with inherently higher crystallographic symmetry, comparison of the quadrupole splitting measured above and below the magnetic ordering temperature can help to determine the easy magnetization direction from spectral data for polycrystalline samples and shed light on the basic *magnetic structure*.

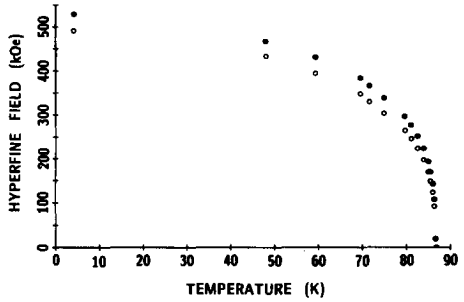

FIG. 6. Temperature dependence of the hyperfine field of $Fe_4(OH)_3(PO_4)_3$. The open and closed symbols correspond to the hyperfine fields measured at the two crystallographically inequivalent iron sites.

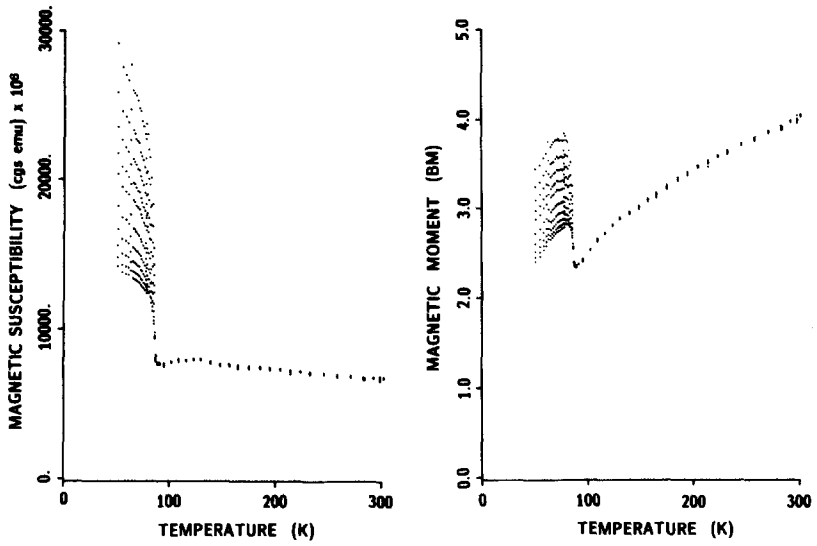

FIG. 7. Temperature dependence of the susceptibility and magnetic moment per iron atom at 10 fields between 0.5 kOe (top) and 5 kOe (bottom) for $Fe_4(OH)_3(PO_4)_3$.

Unfortunately, this is not the case here. The symmetry of the system is low and neither the direction and the asymmetry of the field gradients nor the correspondence between the two doublets above the ordering and the two sextets below that are known with certainty.

Susceptibility Measurements

The susceptibility as a function of temperature for $Fe_4(OH)_3(PO_4)_3$ is shown in Fig. 7 for 10 applied fields between 0.5 and 5 kOe. Extended 3D ordering with a small net magnetization occurs at 86.6 ± 0.3 K in good agreement with the Mössbauer spectroscopy results. The susceptibility is only slightly temperature dependent between the ordering temperature and 300 K and shows a broad maximum at about 125 K. In the present system, *antiferromagnetically coupled dimers* are the most likely source of this behavior, because the exchange interaction between the two iron moments (Fe–Fe intradimer distance is 2.987 Å) coupled through three common oxygen neighbors (i.e., face-sharing octahedra) is assumed much stronger than the interaction between the further iron moments of different but next neighbor dimers (Fe–Fe interdimer distances are 3.53 and 3.72 Å). The presence of a rather strong antiferromagnetic (intradimer) coupling is also supported by the temperature dependence of the magnetic moment per iron atom as defined here by the paramagnetic formula

$$\mu = \left(\frac{3k_B}{N}\right)^{1/2} (\chi T)^{1/2}$$

(Fig. 7). The moment decreases to 2.5 μ_B right above the ordering temperature from 4.2 μ_B at room temperature, a value far below the spin-only value of 5.9 μ_B expected for independent $S = \frac{5}{2}$ ions.

The temperature dependence of the susceptibility of independent dimers of $S = \frac{5}{2}$ ions can be calculated using the formalism described by Smart (*13*). It has a maximum at $\tau = Tk/|J| = 5.79$. Comparing this with the susceptibility maximum at $T = 125$ K, $J/k_B \sim -22$ K (~ -15 cm^{-1}) can be estimated for the exchange interaction between the two moments forming a dimer. The esti-

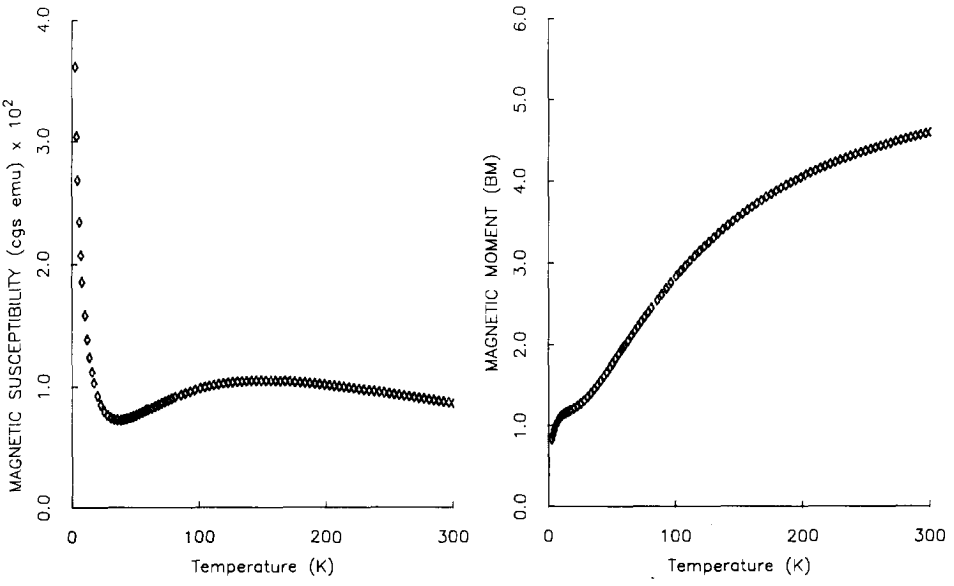

FIG. 8. χ_m and μ vs T (K) for $V_4O(OH)_2(PO_4)_3$.

mated value of $J_{dimer} \sim -15$ cm^{-1} is consistent with the values typically observed for a variety of hydroxy-bridged ferric dimers with Fe–O–Fe bond angles of 90°–110° (*14*). This corresponds to an exchange energy of $2|J|S^2/k = 270$ K, much larger than the ordering temperature of 86.7 K indicating that the exchange interactions responsible for the 3D ordering are much weaker than the interaction between the two members of the dimer. The temperature range studied was too narrow (no data above ambient temperature) and the variation of the susceptibility was too small to perform a more detailed analysis of the susceptibility data as that by the Heisenberg–Dirac–Van Vleck model formula (*15*).

The existence of antiferromagnetically coupled dimers suggests that the three-dimensional ordering is also antiferromagnetic in nature. The obvious remaining net moment below the ordering temperature likely originates from inequivalence of the total moments of the two magnetic sublattices which is expected in a system with low symmetry and based on dimers with inequivalent iron(III) sites. The Mössbauer data also suggest that there is a small difference between the moment of the two different iron sites which may result in weak ferromagnetism. The observed field dependence of χ_m and μ (χ inverse to H_0) at less than $T_{critical}$ is the typical demagnetization effect expected for a weakly ferromagnetic state.

Magnetic susceptibility data have also been determined for the related isomorphous mixed-valence vanadium phase as shown in Fig. 8. The moment vs temperature behavior of this material gives clear evidence of antiferromagnetic exchange, and that is also likely pairwise (dimer) in nature analogous to the iron compound in view of the broad maximum exhibited in χ vs T (~150 K) and the structural isomorphism. The ambient temperature moment of this phase is ~2.3 μ_β/V. Since this material may in fact have truly averaged oxidation states, the concept of individual metal–ion spin states is not well defined. Nevertheless, since the average valence is ~3, we will assume $S = 1$ for comparison pur-

poses. This leads to the expectation of μ_β/V of $\sqrt{8}$ (2.83 μ_β/V) (spin-only behavior) suggesting significant antiferromagnetic exchange at room temperature. The situation with regard to the ultimate lower temperature 3D magnetic ordering of this phase is not as clear as with the iron(III) analog. While μ continues to steadily decrease, the rise in χ_m with decreasing temperature is more reminiscent of the effect of magnetic impurities rather than ordering. On the other hand, possible ordering and/or spin reorientation transitions are suggested by the inflections in μ vs T that are clearly apparent. It is evident that other approaches (e.g., neutron diffraction study) will be necessary in order to obtain a clearer idea of the 3D magnetic ground state of the vanadium system.

Acknowledgments

The authors thank R. S. McLean for susceptibility data on the vanadium compound and C. M. Foris and G. M. Hyatt for the X-ray powder patterns. W.M.R. thanks the National Science Foundation Division of Materials Research, Solid State Chemistry Program Grant DMR 8313710, and the N.U. Biomedical Sciences Grant.

References

1. W. Meisel, H. J. Guttmann, and P. Gutlich, *Corros. Sci.* **23,** 1373 (1983).
2. W. P. Bosman, P. T. Beurskens, J. M. M. Smits, H. Behm, J. Mintjens, W. Meisel, and J. C. Fuggle, *Acta Crystallogr. Sect. C* **42,** 525 (1986).
3. W. Meisel, J. Mintjens, and W. P. Bosman, *J. Phys. Chem. Solids* **49,** 157 (1988).
4. R. Jakeman, A. K. Cheetham, M. Kwiecien, W. M. Reiff, and C. C. Torardi, Inorganic Paper No. 133, *in* "189th ACS National Meeting of the American Chemical Society, Miami Beach, Florida, April 1988" (1988).
5. C. C. Torardi and W. M. Reiff, Inorganic paper No. 115, *in* "Third Chemical Congress of North America, Toronto, June 1988" (1988).
6. P. Main, L. Lessinger, M. M. Woolfson, G. Germain, and J. P. Declerg, "MULTAN 78: A System of Computer Programs for the Automatic Solution of Crystal Structures from X-Ray Diffraction Data," York and Louvain-la-Neuve (1978).
7. N. Walker and D. Stuart, *Acta Crystallogr. Sect. A* **39,** 158 (1983).
8. C. K. Johnson, "ORTEP: A FORTRAN Thermal-Ellipsoid Plot Program for Crystal Structure Illustration," Oak Ridge National Laboratory Report 5138 (1976).
9. C. Cheng and W. M. Reiff, *Inorg. Chem.* **16,** 2097 (1977).
10. R. D. Shannon, *Acta Crystallogr. Sect. A* **32,** 751 (1976).
11. M. L. Lindberg and C. L. Christ, *Acta Crystallogr.* **12,** 695 (1959).
12. L. Katz and W. N. Lipscomb, *Acta Crystallogr.* **4,** 345 (1951).
13. J. Samuel Smart, *in* "Magnetism" (G. T. Rado and H. Shul, Eds.), Vol. III, p. 63, Academic Press, New York (1963).
14. L. Borer, L. Thalken, C. Ceccarelli, M. Glick, J. H. Zhang, and W. M. Reiff, *Inorg. Chem.* **22,** 1719 (1983).
15. R. L. Carlin, "Magnetochemistry," Springer-Verlag, New York/Berlin (1986).